Towards More Accurate Contactless Fingerprint Minutiae Extraction and Pose-Invariant Matching

Hanzhuo Tan, Ajay Kumar
Department of Computing
The Hong Kong Polytechnic University, Hong Kong

Abstract: Contactless fingerprint identification offers significantly higher user convenience, hygiene and has attracted increasing attention for the deployments. However, the presentation of fingers towards the contactless fingerprint sensors is hard to control and often results in unwanted pose changes that significantly degrade the contactless fingerprint matching accuracy. In order to address such problems and improve the fingerprint matching accuracy, this paper proposes a more precise minutiae extraction and pose-compensation approach. As compared with the conventional minutiae extraction approaches, our deep neural network-based approach does not require any image enhancement and is robust to spurious minutiae. All the minutiae extracted from our network are subjected to a three stage pose compensation framework: a) view angle estimation based on the location of core point, b) ellipsoid model formulation which simulates and compensate finger pose, c) intersection area estimation and alignment between different view angles. The proposed ellipsoid model is adaptive to both the silhouette of 2D contactless fingerprint image and the estimated view angle. The corresponding area between the different view angles can be theoretically estimated using this model and incorporated to align two contactless fingerprints for achieving superior matching accuracy. Our reproducible experimental results presented in this paper using public databases, and a database acquired during this work, validate the effectiveness of the proposed framework over the commercial software and earlier methods.

1. Introduction

Automated fingerprint identification is one of the most widely adopted human identity verification systems. Back in 1893, Home Ministry Office, UK, accepted that no two individuals have the same fingerprints [1] and fingerprint was gradually deployed in forensics and law enforcement applications. Uniqueness, persistence [2] and acquisition cost-effectiveness properties of fingerprint win the largest shares on the biometric market. Traditional fingerprint acquisitions require pressing of finger against the scanners hard surfaces and results in elastic distortions which often degrades the matching accuracy [3-5]. More seriously, the latent prints left on the scanner surfaces can be easily lifted and used for sensor-level spoof [6] attacks. On the contrary, contactless fingerprint sensing acquires finger patterns without any physical contact with the scanner and can offer high-quality elastic distortion free images while protecting privacy from residual impressions. Multimodal biometrics systems are known to offer extremely high level of security. It is yet another reason for enhanced research and development interest in this area as the contactless fingerprints can be simultaneously acquired along with other biometric modalities for extremely secured access control.

Earlier work on contactless fingerprint imaging employed a single low-resolution camera [6-11]. Reference [8] details a comparison between the contact-based and contactless fingerprint recognition on 163 fingers and reported superiority of contactless sensor over

contact-based one. Reference [11] investigates identification of very low-resolution contactless fingerprint images by using level-zeros features. With the rapid growth of mobile phone industry, high resolution contactless fingerprints images acquired from smartphones [12]-[14] have been studied for the personal identification. The image formation from the contactless fingers is significantly different from the contacted-based ones. Low-contrast between ridges and valleys details in the contactless fingerprint image are known to result in poor performance using conventional fingerprint image enhancement methods. Secondly, the presentation of fingers against contactless sensors, during acquisition of contactless fingerprints, is often uncontrollable and significantly contributes to the degrade of verification accuracy. As shown in Figure 1, images with different view angles or the poses from the same finger cannot be recognized by a popular COTS (*Verifinger 10.0 SDK* [15]). Therefore, the objective of this work has been to develop a more efficient and accurate minutiae extraction approach, and pose compensation algorithm, to address the limitations of conventional contacted-based minutiae extraction algorithms for the contactless fingerprint identification.

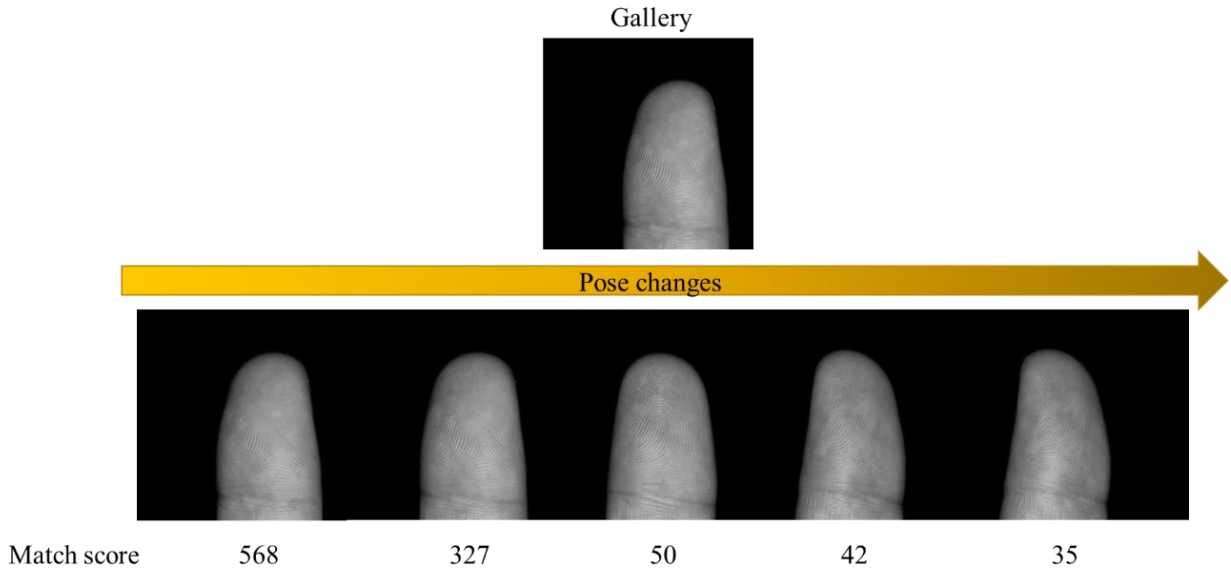

Figure 1: Sample contactless fingerprint image acquired with different finger poses or view angles. The match scores obtained from the *Verifinger*, when the top image is matched with other images at the bottom, is respectively presented with the images. These match scores resulting from different finger poses variations illustrate significant degradations and gradual failure in recognizing contactless fingerprints from the same finger.

1.2. Related Work

1.2.1 Minutiae Extraction

Conventional minutiae extraction algorithms, often require binarized fingerprint ridge images, and can be grouped into two categories. The first group requires enhanced and binarized fingerprint images as input. Morphological thinning or skeletonization techniques are employed on the binarized images and the minutiae positions are localized by detecting pre-

defined patterns [16]. Accuracy of these algorithms rely on the quality of binarized fingerprint images generated from the image enhancement operations, which is another challenging task especially for the low-quality fingerprint images. Typical methods for fingerprint image enhancement include Gabor filtering [17], Short-Term Fourier Transform analysis [18], *etc*. Algorithmic limitations in precisely estimating the ridge frequency, orientation, or illumination profile for the fingerprint image enhancement algorithms often result in distortions in the enhanced fingerprint images. Furthermore, due to the intrinsic irregularity of ridge patterns, thinning or skeletonization operations can easily generate spikes and introduce spurious minutiae [1]. In order to alleviate such limitations from the enhancement, direct extraction of fingerprint minutiae from the raw input or fingerprint images has been investigated. Reference [19] investigated the ridge flow lines from the orientation fields to localize the minutiae. However the requirement of reliable orientation prediction and its sensitivity to the (varying) pixel intensity pose limitations to the robustness of this algorithm. Some other traditional direct minutiae extraction methods [20]-[21] are also known to be sensitive to the noise and not suitable for practical deployments and enhance-thinning-extract trilogy is accepted as the standard.

Successful usage of deep convolutional neural networks for a range of computer vision problems has motivated researchers to directly predict the fingerprint minutiae using trained networks. Several promising attempts have emerged in the literature that provide raw fingerprint images to a trained deep neural network and directly obtained minutiae as the output. Reference [22] details such investigation which partitions the input images into multi-scale patches and trained a neural network to learn the label of each patch. Similarly, [23] also employs a patch-based prediction but introduces *JudgeNet* for the prediction on the existence of minutiae, and *LocateNet* to recover the precise minutiae locations. On the other hand, there are also interesting examples where the entire fingerprint image is employed to predict the minutiae score map. Reference [24] adapts a loss function, with domain or prior information, to extract the minutiae while [25] trains a fully convolutional network to recover minutiae from latent fingerprint images. More promising results using a two-stage architecture, *i.e*., a *CoarseNet* to get initial results and *FineNet* to consolidate such predictions, appear in [26] but for the latent fingerprint images.

Although considerable efforts have been devoted into the contact-based fingerprint minutiae extraction, research on the contactless fingerprints has received very little attention. All earlier work in this area has adapted the enhance-thinning-extract trilogy standard inherited from the contacted-based fingerprint systems for contactless fingerprint minutiae extraction.

Reference [9] details homomorphic filter-based approach for the contactless fingerprint enhancement while [27] adopts intrinsic image decomposition and image filtering with the improved Gabor filters for the enhancement. Similar to the conventional contacted-based fingerprint methods, these algorithms suffer from the spurious minutiae and enhanced fragility to the low-contrast images. Furthermore, none of earlier methods for the contactless minutiae extraction attempted any cross-database evaluation and comparison with COTS.

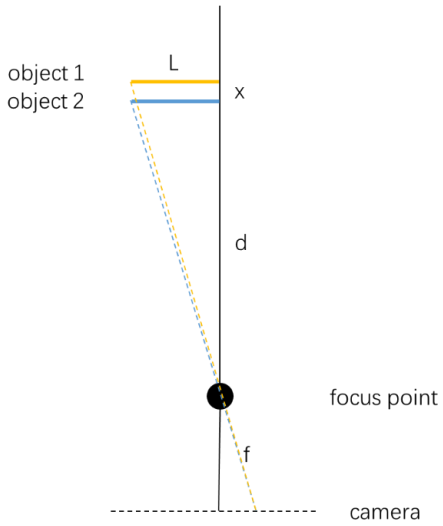

Figure 2: Illustration for the perspective projection. The focal length is represented by f while the object 1 and object 2 are of *same* size L but placed at distances d and $(d + x)$ from the focus point. The projected size on the camera for object 1 is $L \times (f/d)$ while the projected size for object 2 is $L \times (f / (d + x))$. When d is significantly larger than x as is common during the contactless fingerprint acquisitions, for example d=10 cm, x=0.5 cm, the projected size ratio between the details from object 1 and object 2 is 0.95:1, which is negligible as compared to the degradation caused by the view angle changes.

1.2.2 Pose-Invariant Fingerprint Recognition

Contactless fingerprint identification performance is highly sensitive to the pose-changes which are more frequent due to the nature of imaging. Almost all earlier attempts [7]-[8] in the literature have preferred to reject or eliminate contactless fingerprint images with large poses. Reference [28] however provided a promising investigation on the need for such pose compensation and referred this problem as perspective distortion. Nevertheless, such problem may not be related to the 'perspective distortion' as this term is widely known to relate the objects size differences presents on the acquired images, with respect to the distances between objects and camera. As shown in Figure 2, the distance between finger and sensor is significantly larger than the finger size, hence the effect of perspective distortion is expected to be negligible. Instead, the degradation in performance is largely attributed to the finger pose. It is worth noting that for the face recognition problem, the registration of human faces towards the front view is referred as the face frontalization [29]-[30]. In this context, we use the term view angle or pose compensation to address similar problem during the contactless fingerprint

identification. In [28], view angle is compensated by simulating the rotation of finger. The top-view undistorted finger image was projected to a 3D model and simulated rotation in 3D space, followed by its back projection to 2D space for recovering the template for distorted image. During the recognition, view angle was first predicted by neural network for each query image, before matching with the corresponding registered template. This is a promising work but only considered small view angles, *i.e*. within 20 degrees, and evaluated on a private database.

1.3 Our Work and Contributions

This paper investigates the problem of precise minutiae extraction and pose compensation for to achieve more accurate contactless fingerprint identification. A deep neural network based direct minutiae extraction is proposed to address limitations of conventional enhance-thinning-extract trilogy methods for the frequently acquired low-contrast contactless fingerprints. Our neural network uses raw contactless fingerprint image patches as the input to *directly* predict minutiae label and its orientation. In order to ensure robustness against scale across databases, atrous spatial pyramid pooling is adopted to generate appropriate reception field from the single input. Each of the extracted minutiae are subjected to the pose compensation framework based on the proposed ellipsoid model which offers several benefits over the polynomial model in [28]. Firstly, in comparison to the estimation by a trained neural network in [28], the view angle or pose of input finger sample can be mathematically computed from the distance ratio of core point towards the two boundaries in our ellipsoid model. In addition, proposed ellipsoid model can theoretically simulate the large finger poses while in [28] such situation was not considered. Furthermore, the alignment between different view-angle contactless finger images is investigated in ellipsoid model. As shown in Figure 3, only the intersection regions between side-view and top-view fingerprint image can be matched, while other areas will remain invisible in another image, and therefore degrade the recognition accuracy recognition.

The main contributions from this paper can be summarized as follows:

1. This paper develops a deep neural network-based minutiae extraction framework for the contactless fingerprint images. In the best of our knowledge, this is the first direct contactless fingerprint minutiae extraction method and with the cross-database performance evaluation. Our reproducible experimental results in section 4 indicate that this method is robust to public database without any fine-tuning or re-training requirements. Trained with only small labeled data, our model also achieves superior performance over COTS.
2. This paper develops a three stage pose compensation framework, based on ellipsoid

model, to address pose-invariant contactless fingerprint identification problem. The proposed framework can mathematically estimate and compensate for the varying finger poses. Our comparative experimental results presented in this paper illustrate significant improvement from the proposed framework.

3. This work also developed a new database of contactless 2D fingerprint images with large pose variations. We provide 40 manually labeled orientations and 140 labeled minutiae samples together with this database. This database consists of 1400 contactless fingerprint images acquired from 140 fingers and is made publicly available [45] to encourage much needed research in this area.

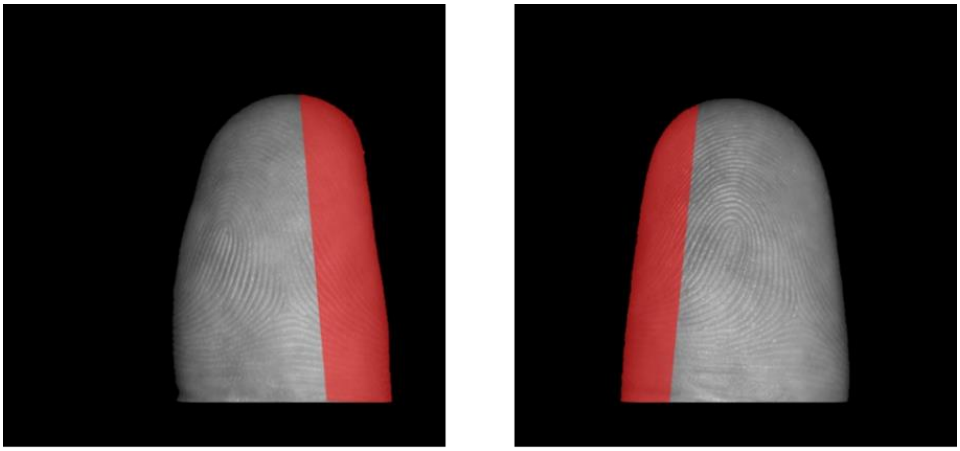

(a) (b)

Figure 3: Sample real contactless fingerprint images acquired under with two poses. The red part in sample (a) is invisible in (b), while the red part in (b) is invisible in (a).

The rest of this paper is organized as follows. Section 2 introduces our pose compensation framework for the contactless fingerprint images. Section 3 details the minutiae extraction network developed in this work for the contactless fingerprints. The details on all the experiments, along with newly developed contactless fingerprint databases with large pose changes, are presented in section 4. Key conclusions from this paper and further work directions are summarized in section 5 of this paper.

2. Contactless Fingerprint Pose Compensation

High degree of freedom available to the users, during the contactless fingerprint image acquisition, often results in contactless fingerprint images with varying poses and such pose changes are known to degrade the matching accuracy (Figure 1). Therefore this section systematically develops and introduces a pose compensation approach which is employed for more accurate contactless fingerprint identification. The minutiae extraction from such pose compensated images is performed by *ContactlessNet* and detailed in section 3.

2.1 Ellipsoid Model for Contactless Fingerprint

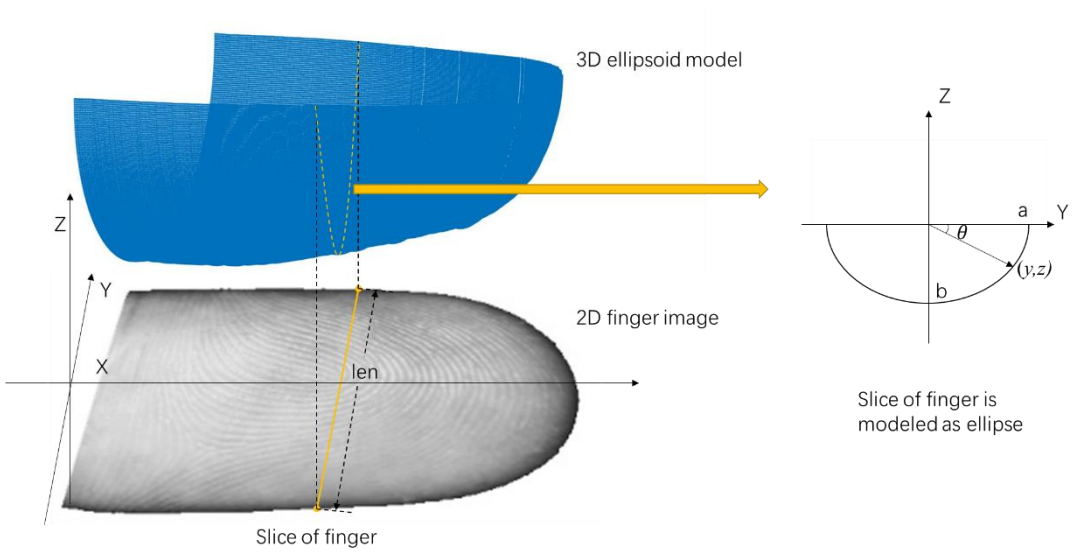

Figure 4: Contactless fingerprint formation using ellipsoid model.

In this paper we model contactless fingerprint image formation using a 3D elliptical (ellipsoid) surface. Such modelling is largely based on our observation that each slice of finger is more likely to be an ellipse with about 1.2 ratio between the major and minor axis. This is unlike earlier work in [28] which modeled the finger surface using a third order polynomial function. Figure 4 illustrates the contactless image formation using such 3D ellipsoid model, with each slice of ellipsoid as an ellipse with a and b as the major and minor axis respectively. Such parameterized ellipse function can be described as in the following:

$$y = a * \cos(\theta)$$
$$z = b * \sin(\theta) \quad (1)$$

where

$$a = len/2$$

The major axis a can be computed from slice length (*len*) observed in the fingerprint image.

2.2 View Angle Estimation

The pose changes along the Y axis can be conveniently compensated by the image rotation. As the finger movement along Z axis is barely trackable from a single image, the pose compensation framework in this work is focused on changes along the X axis. Let α be the view or rotation angle, the new coordinates for each of the slice of ellipsoid can be computed as follows:

$$y' = y * \cos(\alpha) - z * \sin(\alpha) = a * \cos(\theta) * \cos(\alpha) - b * \sin(\theta) * \sin(\alpha)$$
$$z' = y * \sin(\alpha) + z * \cos(\alpha) = a * \cos(\theta) * \sin(\alpha) + b * \sin(\theta) * \cos(\alpha) \quad (2)$$

According to sum-to-product identities, i.e., $\cos(\theta) * \cos(\alpha) - \sin(\theta) * \sin(\alpha) = \cos(\theta + \alpha)$, y' and z' can be simplified into:

$$y' = a * \cos(\theta) * \cos(\alpha) - b * \sin(\theta) * \sin(\alpha) = A * cos(\theta + B)$$
$$z' = a * \cos(\theta) * \sin(\alpha) + b * \sin(\theta) * \cos(\alpha) = C * cos(\theta - D) \quad (3)$$

where

$$A = \sqrt{(a * \cos(\alpha))^2 + (b * \sin(\alpha))^2}$$
$$B = arctan\frac{b * \sin(\alpha)}{a * \cos(\alpha)}$$
$$C = \sqrt{(a * \sin(\alpha))^2 + (b * \cos(\alpha))^2}$$
$$D = arctan\frac{b*\cos(\alpha)}{a*\sin(\alpha)} \quad (4)$$

For each slice of 3D ellipsoid model, A is half the length of slice computed from the acquired contactless fingerprint image. The view or rotation angle can be estimated as in the following discussion:

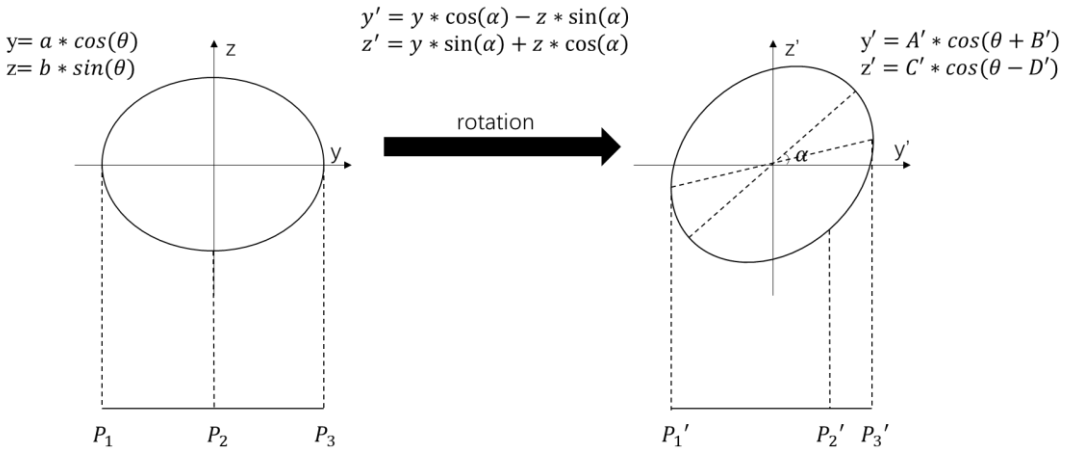

Figure 5: Contactless fingerprint rotation angle estimation.

In Figure 6, P_1, P_2, P_3 are the projection of left, center and right point of ellipse, after rotation, P_1', P_2', P_3' are the corresponding points respectively. From the ratio of $P_1'P_2'$ to $P_2'P_3'$, required rotation angle can be estimated using the following geometrical relationship.

$$P_1'P_2' = A' + A' * \cos(-\frac{pi}{2} + B')$$
$$P_2'P_3' = A' - A' * \cos(-\frac{pi}{2} + B')$$
$$ratio = \frac{P_1'P_2'}{P_2'P_3'} = \frac{1 + \cos\left(-\frac{pi}{2} + B'\right)}{1 - \cos\left(-\frac{pi}{2} + B'\right)}$$
$$B' = arctan\frac{b*\sin(\alpha)}{a*\cos(\alpha)} \quad (5)$$

This *ratio* can be directly estimated from contactless fingerprint images as shown in Figure 6.

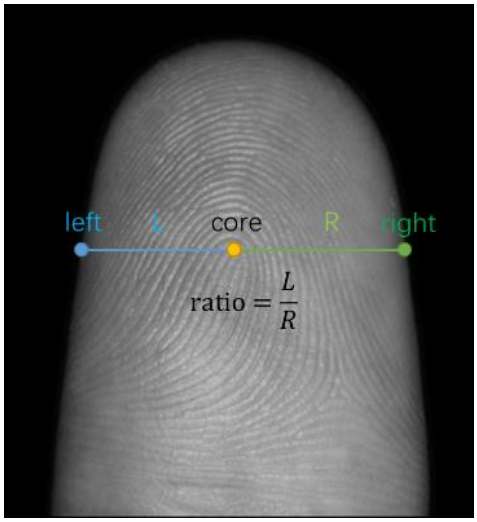

Figure 6: Keypoints and ratio estimation from a fingerprint image.

2.3 Pose Compensation

Each slice of finger, as shown from the left-hand image in **Figure 7**, can be represented using as an ellipse segment in the 3D space. Corresponding 2D slice P_1P_3 is a row of pixels in the 2D contactless fingerprint image. For each of the transfer points in P_1P_3 to $P_1'P_3'$, forward pose compensation is performed. The forward pose compensation is summarized as in Algorithm 1.

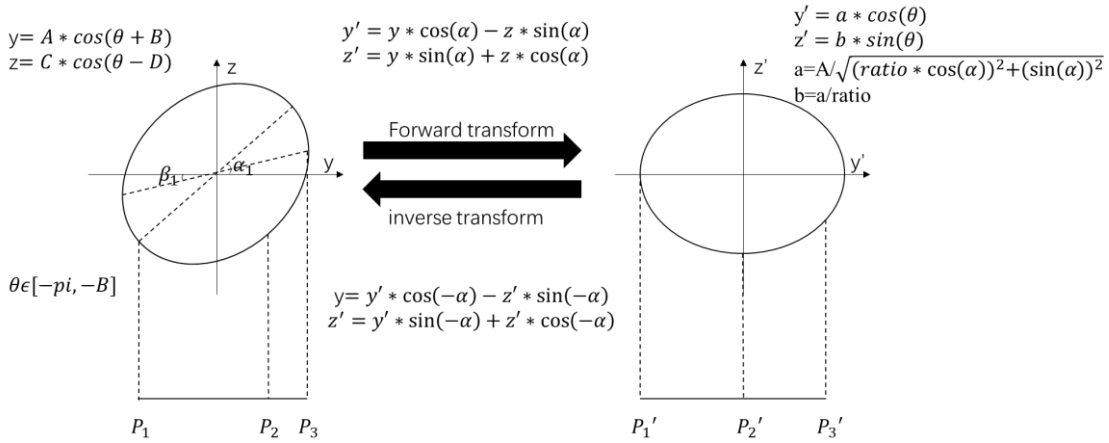

Figure 7: Contactless fingerprint Pose compensation.

Algorithm 1: Forward pose compensation
Input: Minutiae
Output: Pose compensated minutiae

1. Estimate view angle α using (5)
2. **for** each minutia with index (x, y, θ) **do**
3. Compute finger length *len* from x^{th} row on contactless fingerprint image
4. Estimate parameters for corresponding ellipse model using (4)
5. Compute depth coordinate z using (3)
6. Rotation transformation of (y, z) using (2) to compute new y'
7. Return (x, y') as compensated coordinate for the minutiae
8. **end for**

The Algorithm 1 can be easily adapted for the image formulation, nevertheless, the forward image transformation will result in floating coordinate values. The conversion of float coordinate into the integer coordinate can inevitably degrade the image quality and generate blurring. In order to address such adverse influence, inverse pose compensation which is designed for the image is summarized as in Algorithm 2.

Algorithm 2: Inverse pose compensation
Input: Contactless fingerprint image
Output: Pose compensated contactless fingerprint image

1. Estimate view angle α using (5)
2. **for** each row x' in the pose-compensated image **do**
3. Compute finger length *len* in x^{th} row of contactless fingerprint image
4. Estimate parameters for corresponding ellipse model using (4)
5. Compute major axis $a = A/\sqrt{(ratio * \cos(\alpha))^2 + (\sin(\alpha))^2}$ and minor axis $b = a/ratio$
6. **for** each column y' in pose-compensated image **do**
7. Compute depth coordinate z' using (3)
8. Rotation transformation of (y', z') using (2) with $-\alpha$ and compute y
9. Return pixel value of (x, y) as the pixel value for (x', y')
10. **end for**
11. **end for**

2.4 Alignment for View Angle Variations

A sample contactless 2D fingerprint image acquired with pose or view angle of α°, as shown in Figure 8(a), needs to be registered into the front-view image in Figure 8(b) acquired during the user enrollment. After such pose compensation, the region PQ of contactless finger slice in Figure 8(a) will be transferred to the region to region $P'Q'$ of finger slice in Figure 8(b). However, in contactless fingerprint image acquired with sensor view angle as in Figure 8(b), the region $P'Q'$ is not available or visible. Similarly, the region RS is not visible in the image in Figure 8(a) or the contactless fingerprint image acquired from the camera view angle of α°. Therefore, after the pose compensation, the corresponding region $R'S'$ in pose compensated image in Figure 8(b) will have not have any details or the contents. In summary, $Q'R'$ will be the pose compensation result for the contactless fingerprint image acquired in Figure 8(a).

Similarly for another contactless fingerprint image acquired with another view angle φ°, as shown in Figure 9(a), the pose compensation result will be $U'V'$. Under a generalized assumption or for direct matching between contactless fingerprint image in Figure 8(a) and Figure 9(a), the alignment between images with view angle α° and φ° is shown in Figure 10. The intersection between these two contactless fingerprint images from different view angles is the region $U'V'$ while region $V'R'$ is not visible in the fingerprint image acquired with α°

view angle. Therefore, only the intersection or common region $U'V'$ will be retained for the matching.

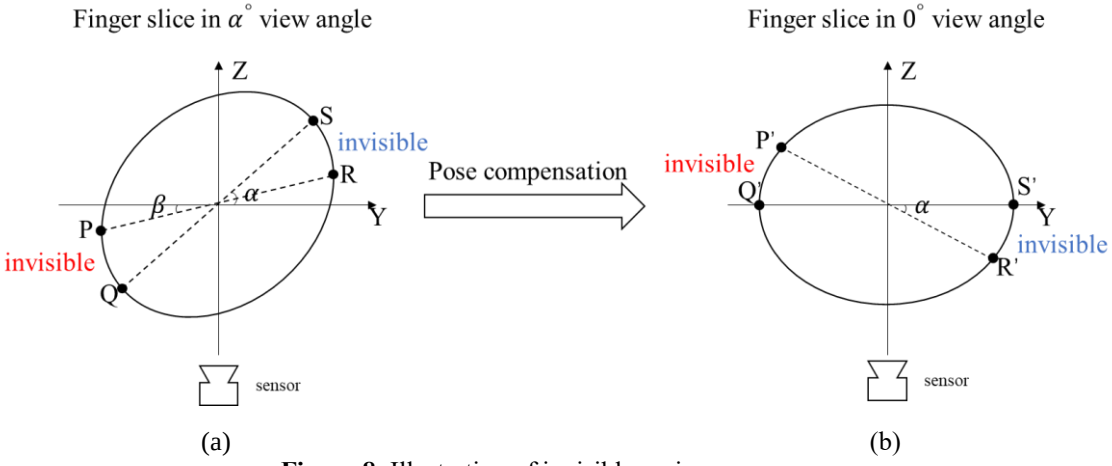

Figure 8: Illustration of invisible regions: case one.

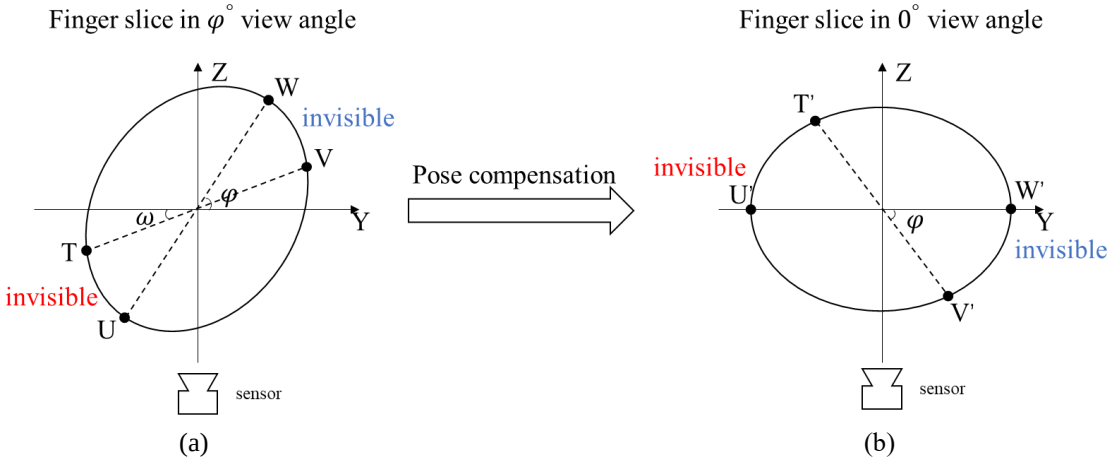

Figure 9: Illustration of invisible regions: case two.

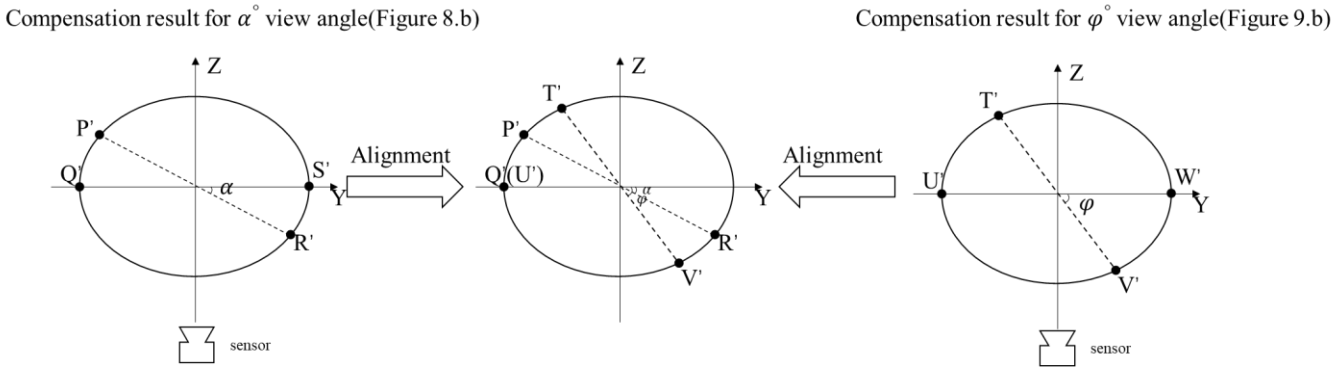

Figure 10: Illustration of alignment between two contactless fingerprint images, from the same finger, acquired under different view angles.

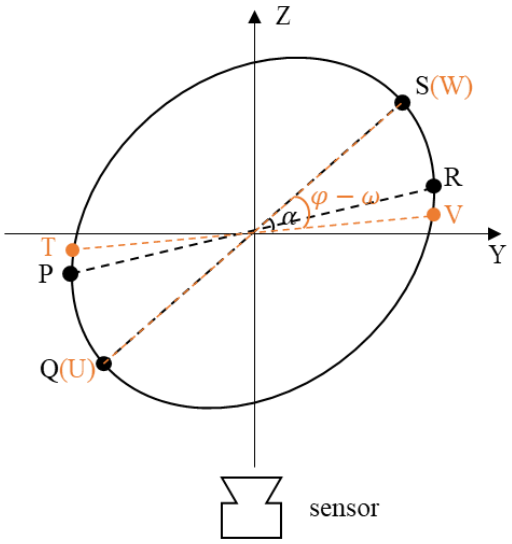

Figure 11: Aligned region of interest estimation from two contactless fingerprint images.

In order to estimate the corresponding region *QV in* the contactless fingerprint image acquired with α° view angle, firstly the finger image acquired with view angle of φ° is aligned into it as shown in Figure 11. We can use equation (3), i.e. $y = A * cos(\theta + B)$, $z = C * cos(\theta - D)$, to locate any such point (*y, z*) on corresponding region *QV*. The point *V* on contactless fingerprint surface in Figure 11 can be localized using the following geometrical relationship:

$$\tan(\alpha - (\varphi\text{-}\omega)) = \frac{z}{y} = \frac{C * \cos(\gamma - D)}{A * \cos(\gamma + B)} \tag{6}$$

Since point Q is located on ellipse surface corresponding to $\theta = -180^{\circ}$ and point V at $\theta = \gamma^{\circ}$, the corresponding intersection region QV is localized at ellipse surface with $\theta\epsilon[-180, \gamma]$. However for fingerprint image acquired with φ° view angle, these corresponding region QV are located on surface corresponding to $\theta\epsilon[-180, -B]$ since $\theta = -B^{\circ}$ represents the point G or the point with largest y coordinate. Figure 12 summarizes the computation for intersection regions corresponding to cases with contactless fingerprint images acquired from different view angles are matched.

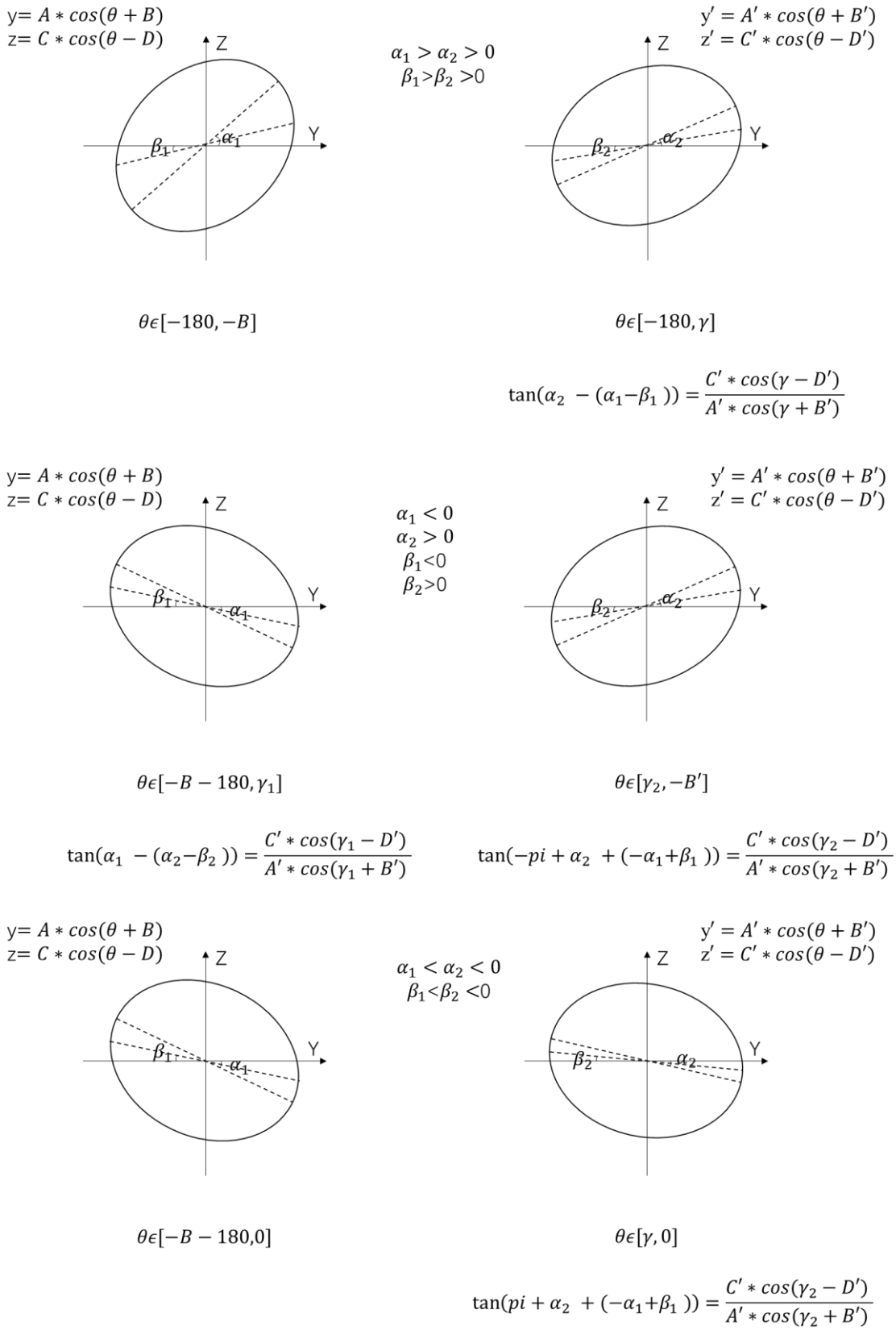

Figure 12: Intersection region estimation for different view angle cases.

With proposed alignment approach, the final pose compensation and matching framework for a pair of minutiae is summarized as Algorithm 3. It should be noted that inverse pose

compensation and matching for the images is similar to Algorithm 3.

Algorithm 3: Pose compensation and matching
Input: Minutiae template T_1 and minutiae template T_2
Output: matching score

1. Estimate view angle α, φ for minutiae template T_1, T_2 using (5)
2. **for** each minutia (*x, y, theta*) in template T_1 **do**
3. On original contactless fingerprint image, count the finger length L in x^{th} row
4. Compute parameters of corresponding ellipse model using (4)
5. Compute the θ range w.r.t φ as in Figure 12
6. **if** corresponding *theta* of coordinate y is in computed θ range
7. Compute depth coordinate z using (3)
8. Perform rotation transform of (y, z) using (2) and get new y'
9. Save (x,y') as compensated coordinate for the minutia
10. **end if**
11. **end for**
12. Repeat step 2-11 for minutia template T_2, replace φ with α in step 5
13. Perform matching between the compensated templates

3. Contactless Fingerprint Minutiae Extraction

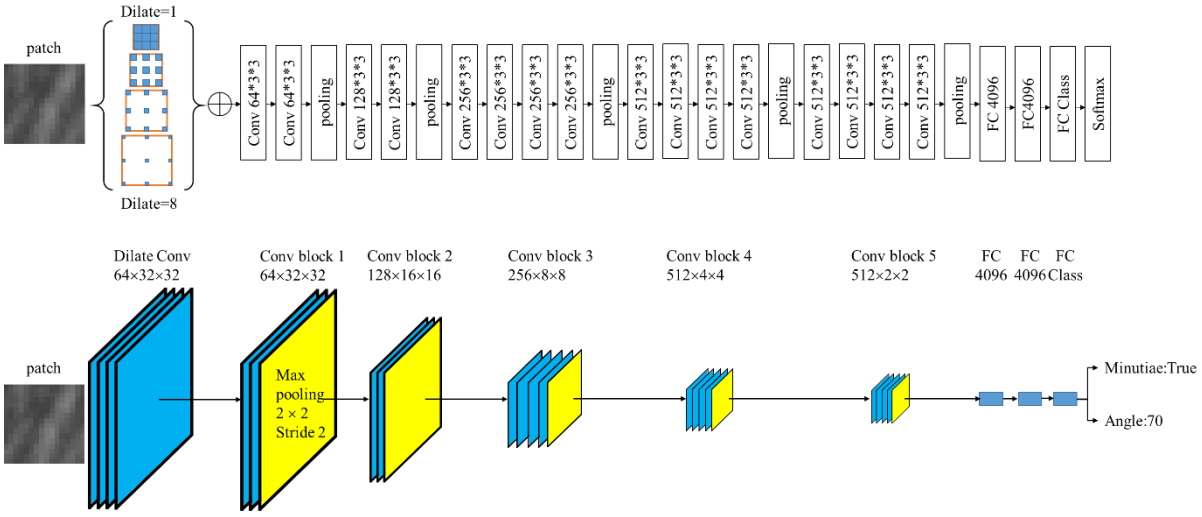

Figure 13: The architecture for *ContactlessNet* (top) with the illustration of corresponding output sizes (bottom).

This section details deep neural network architecture developed to more precisely extract the minutiae features from the contactless fingerprint images. This framework is referred to as *ContactlessNet* and illustrated in in Figure 13. Each of the Conv block shown in this figure includes a convolutional layer, batch normalized layer, *ReLu* layer and dropout layer. Contactless fingerprint frequently illustrates scale changes due to the nature of contactless imaging and therefore the network with multiple or dilated kernels was preferred. In order to

address the limitations caused by the availability of very limited labelled data, patch-based network was adopted. The minutia extraction process from a raw contactless fingerprint image includes: (a) extraction of a $N \times N$ patch for each center pixel, (b) generation of a minutia label and orientation for each patch using the trained network, (c) refining and suppression of spurious minutiae.

3.1 Patch Generation

Unlike several latent fingerprint databases which provide latent fingerprint images with corresponding minutiae data (ground truth) labelled by human experts, there is no such public contactless fingerprint database with labelled minutiae available so far. Largely due to the complexity associated in the formation of contactless fingerprint images, the synthetic fingerprint images [31] cannot be generated and used as training sample as in [32]. In order to address problems due to the availability of limited data, a patch-based minutiae location and orientation prediction approach was adopted. We extract a $N \times N$ image patch, centered at every image pixel in contactless fingerprint image. The labelled contactless fingerprint images are also augmented by scaling, rotation and the luminance adjustments. Furthermore, for each minutia point, its surrounding M × M pixels are also labelled as potential minutiae points.

3.2 Minutiae Extraction and Orientation Prediction

ASPP [33] is introduced to improve network robustness towards scale especially for cross-database evaluation. By concatenating dilated convolutional layers with different dilation factors, ASPP provides multi-scale reception fields for later layers without increasing the depth of architecture. In minutia extraction, each patch has a label of 0 for non-minutia point, and 1 for minutia point. As for orientation prediction, the regression problem is translated into a classification task. The orientation range is discretized into L different values which are fixed empirically for orientation prediction, it uses the same network architecture as shown in Figure **13** but trained trained separately. Once the minutia is detected, the patches centered at each minutia locations are subjected to the orientation prediction using separately trained network. Our experiments indicate that the usage of single network to predict minutia label with orientation can also achieve similar results. However, we preferred to use separate networks to avail computational advantages.

3.3 Refinement and Suppression of Spurious Minutiae

Detecting or eliminating spurious minutiae is essential component of postprocessing operations

in the conventional fingerprint algorithms. We also incorporated refinement of the network outputs to achieve similar objectives. Therefore to alleviate the possibility of detecting spurious minutia, only the predicted minutia score with the probability over 0.9 is accepted. Furthermore, as in the database, fingerprint ridge distance is estimated about 8 pixels. Therefore, it is expected that within one ridge distance only single minutia can exist. Only the predicted minutia with highest probability will be considered as the final minutia point within the one ridge distance.

4. Experiments and Results

This section provides details on all the experiments that were performed to ascertain the robustness and effectiveness of proposed minutiae extraction and pose compensation framework for the contactless fingerprint images. We firstly introduce the public databases used in this work, which includes the database developed from this work, and outline experimental protocols. This is followed by the experimental results for the minutiae extraction in section 4.2 and pose compensation in section 4.3.

4.1 Contactless Fingerprint Databases

We employed publicly available contactless fingerprint databases from [34] and [35] for our experiments. However, lack of publicly available contactless fingerprint database with large number of pose changes, like commonly observed from user interaction during contactless finger imaging, motivated us to acquire a new database for this research. Therefore, a database consisting of 1400 contactless fingerprint images from 140 different fingers was acquired from the volunteers in our university. Ten fingerprint image samples were acquired from each of the client fingers. The images were acquired using a handheld camera. Unlike for the other publicly available contactless fingerprint databases, a significant amount of pose variations was ensured during the image acquisition. Each of the users were suggested to rotate their fingers during the image acquisition process and the images were acquired under the ambient illumination in indoor environment. Such (intentional) requirements is expected to degrade image consistency or the quality but helps to simulate the real-world contactless fingerprint image acquisition process, as neither illumination conditions nor the user behavior is predictable. The distance between the camera and finger was about 15 cm and the fingers were rotated from the left to right direction for acquiring fingerprints with ten different poses. In addition to this database, reproducible experimental results are also presented using two public contactless fingerprint

databases from [34] and [35]. Figure 14 shows sample images from three contactless fingerprint databases.

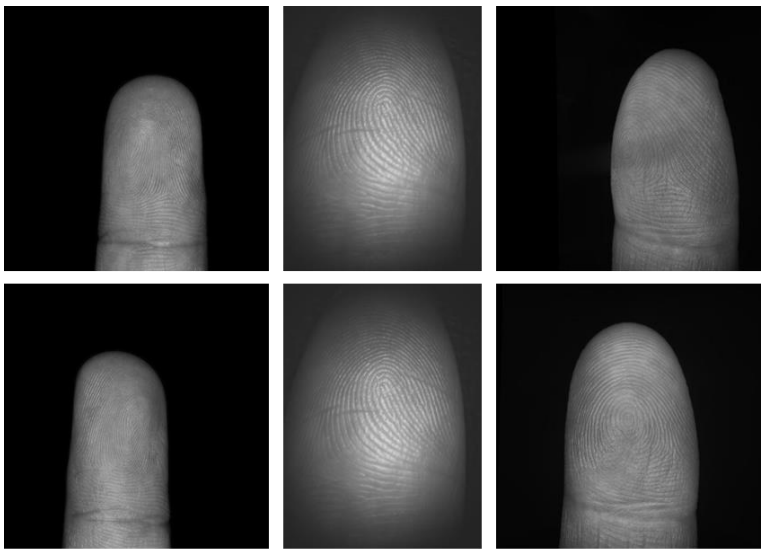

Figure 14: Samples images from three contactless fingerprint databases: (a) from this work, (b) from database in [34], and (c) from database in [35].

In order to perform fair comparison with *Verifinger* [15] or the COTS and NBIS [36], the original images acquired from the three databases should be down sampled, similar to as in earlier works, *e.g.* [37]. This is largely due to the fact that these algorithms are designed or optimized to accept contact-based fingerprints from the FBI compliant fingerprint sensors, which usually have much smaller sizes as compared to contactless fingerprint images in public databases. The scale or down-sampling factor is determined by the nature of images, in widely used public databases [38], [39], which have ridge distance around 8 pixels. In this work, all contactless fingerprint images are therefore also down sampled to represent ridge distances in about 8 pixels with resolution of 400 × 400 pixels and 500 dpi.

The *ContactlessNet* in this work was trained from 40 images with manually marked minutiae locations and orientations. This contactless database was acquired from 140 different clients (fingers) and each of the clients provided 10 different samples. In order to train *ContactlessNet*, the images from last 20 client fingers were selected as the training set and were manually labelled, *i.e.* each client finger with 2 labelled samples and therefore a total of 40 images for the training. In order to ensure training and test set separation, these 20 fingers are excluded from *all* the matching experiments. Therefore, the rest of 120 different client fingers, each with 10 samples, or a total of 1200 (120×10) images, are used for the performance evaluation. The manually labelling operation is quite time-consuming and therefore only small (40) number of images were labelled and made available via [45]. The average number of

minutiae marked on each of such labeled contactless fingerprint images is 47.5. There's no fine-tuning or re-training for the performance evaluated on databases in [34], [35] and only 40 training images are employed from the database acquired in this work. In order to achieve illumination normalization, each of the contactless fingerprint images were subjected to adaptive histogram equalization [40]. The experiments to evaluate the effectiveness for the minutiae extraction performance are performed in two stages. First, we ascertain the accuracy in the minutiae detection or perform direct minutiae extraction evaluation. These experiments use 100 images acquired in this work which were randomly selected and labelled or marked (accessible from [45]). Besides, 50 images are randomly selected and marked from each of the databases in [34] or [35]. Comparative performance evaluation for the minutiae extraction was performed on these 200 test samples. During the second stage, we ascertain the matching accuracy using the verification and the recognition performance using Receiver operating characteristic (ROC) and Cumulative Matching Characteristic (CMC) respectively. The performance from the pose compensation approach is similarly evaluated using the verification and recognition performance.

The core point detection follows the same track of minutiae extraction, *i.e*. patch-based detection, with a 8-layer convolutional neural network trained on the same 20 client finger images, each with 10 manually marked samples. The data augmentation is incorporated using scaling, luminance adjustment and the rotation. The patch size for the core point network was empirically set as 64×64. The architecture for core point detection network is summarized in the following table, where *Conv* stands for convolutional layer, BN represents batch normalization layer, Relu is activation function, Drop denotes dropout layer while FC denotes fully connected layer.

Table 1: Core point detection network.

Layer	Filter Size	Output Number	Stride
Conv_BN_ReLu_Drop	3	32	2
Conv_BN_ReLu_Drop	3	32	1
Conv_BN_ReLu_Drop	3	64	2
Conv_BN_ReLu_Drop	3	64	1
Conv_BN_ReLu_Drop	3	128	2
Conv_BN_ReLu_Drop	3	128	1
Conv_BN_ReLu_Drop	3	256	2
Conv_BN_ReLu	3	256	1
FC		2	

The database [34] is used to generate seven synthetic 2D contactless fingerprint images, corresponding to different view angles, to simulate the random placement of finger, as in [41]. These synthetic data are also employed for the performing evaluation. We employ a total of 96 3D fingers to generate 672 contactless 2D fingerprint (synthetic) images. A sample 3D (view)

fingerprint and its corresponding seven 2D contactless 2D fingerprints, observed from different view angles, are shown in Figure 15.

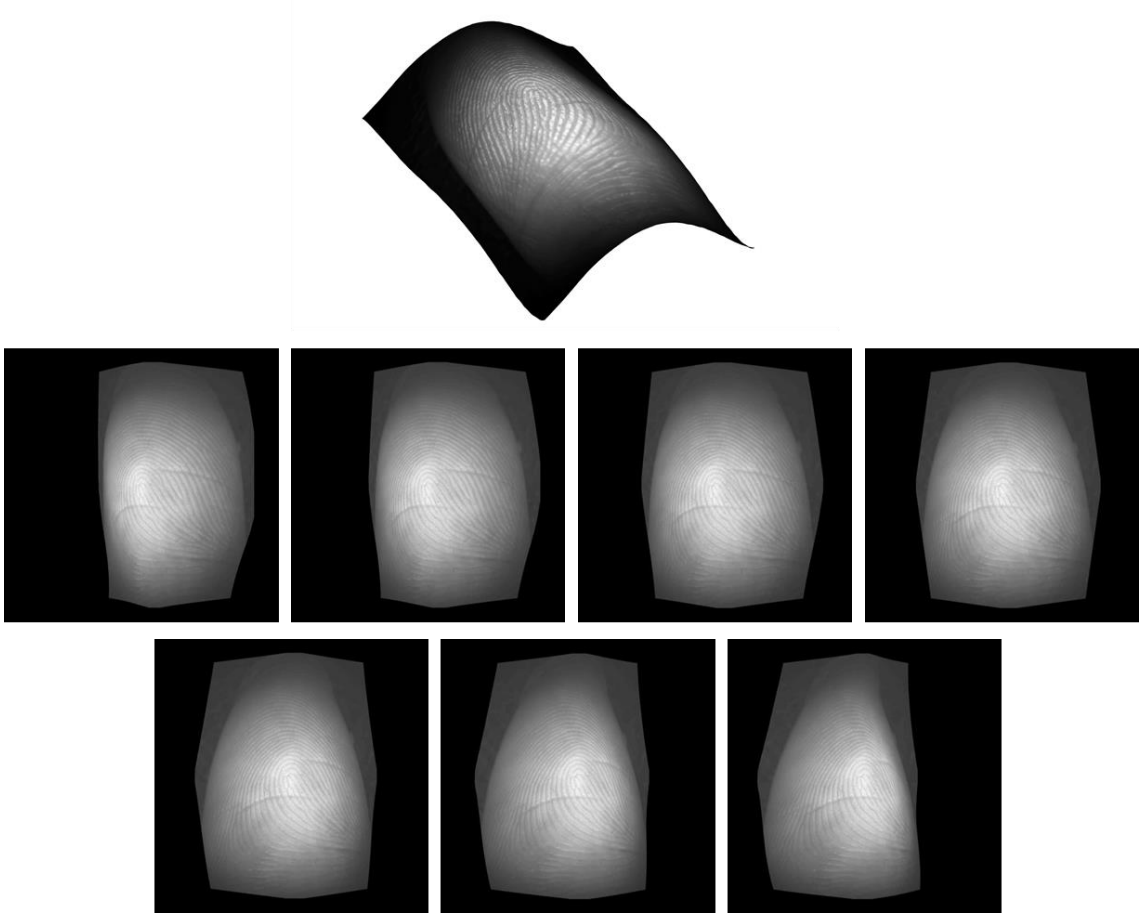

Figure 15: Sample 3D fingerprint image from [34], the 3D view of fingerprint presented on top left and rest are synthetic fingerprint image from view angle of 60 to 120 degrees with 10 degrees interval respectively.

4.2 Contactless Fingerprint Minutiae Extraction

The network detailed in section 3 empirically fixed patch size N as 32, potential minutiae range M as 5, and orientation directions L as 90 for all the experiments in this work. The results from the direct evaluation of the minutiae detection accuracy using the precision, recall, and the F1 measure are summarized in Table 2. These evaluation metrics for the minutiae detection have also been used in earlier works but for the latent fingerprints, *e.g*. [24]. If the distance between the recovered minutia and a manually labelled minutia is within 8/16 pixels, which is about a one/two ridge distance, the recovered minutia is considered as a true minutia. It should be noted that this is a one-to-one matching, *i.e*. each of the ground truth minutia should only be matched with one predicted minutia. Comparative experimental results from the COTS (*Verifinger* [15]), open source extractor MINDTCT from NBIS [36], and using a VGG [42] network are also presented in this table. All experiments using deep neural networks employed Pytorch [43] and were run on Nvidia GTX GeForce 1080Ti.

In addition to direct minutiae extraction performance evaluation, we are attempted to evaluate the verification performance to further ascertain the effectiveness of the proposed approach. Such verification experiments generated 5400 (120 × 45) genuine and 71400 (1190×1200/2) imposter match scores from the database acquired during this work, 2016 (96×21) genuine and 223440 (665×672/2) imposter scores using the synthetic data generated followed [41], and 8524 genuine and 51814054 imposter match scores using all available 2D contactless images from the database in [35]. Minutiae Cylinder Code [44] is used to ascertain the matching performance from the extracted minutiae (using the methods in Table 2). The

Table 2: Comparative results from different methods for the minutia extraction using different databases.

Distance		8 pixels			16 pixels		
Database	Method	Recall	Precision	F1	Recall	Precision	F1
Database acquired during this work [45]	MINDTCT	0.129	0.195	0.151	0.272	0.412	0.323
	Verifinger	0.393	0.338	0.359	0.553	0.475	0.506
	VGG	0.716	0.684	0.694	0.762	0.728	0.740
	ContactlessNet	**0.759**	**0.733**	**0.741**	**0.790**	**0.764**	**0.772**
PolyU Contactless Fingerprint Database [34]	MINDTCT	0.124	0.100	0.106	0.307	0.248	0.269
	Verifinger	0.353	0.425	0.381	0.496	0.597	0.537
	VGG	0.653	0.558	0.597	0.704	0.601	0.644
	ContactlessNet	**0.664**	**0.604**	**0.628**	**0.704**	**0.640**	**0.665**
Benchmark 2D/3D Fingerprint Database [35]	MINDTCT	0.07	0.144	0.093	0.188	0.372	0.246
	Verifinger	0.332	0.502	0.395	0.447	0.677	0.534
	VGG	0.596	0.643	0.614	0.644	0.695	0.663
	ContactlessNet	**0.654**	**0.701**	**0.672**	**0.691**	**0.741**	**0.710**

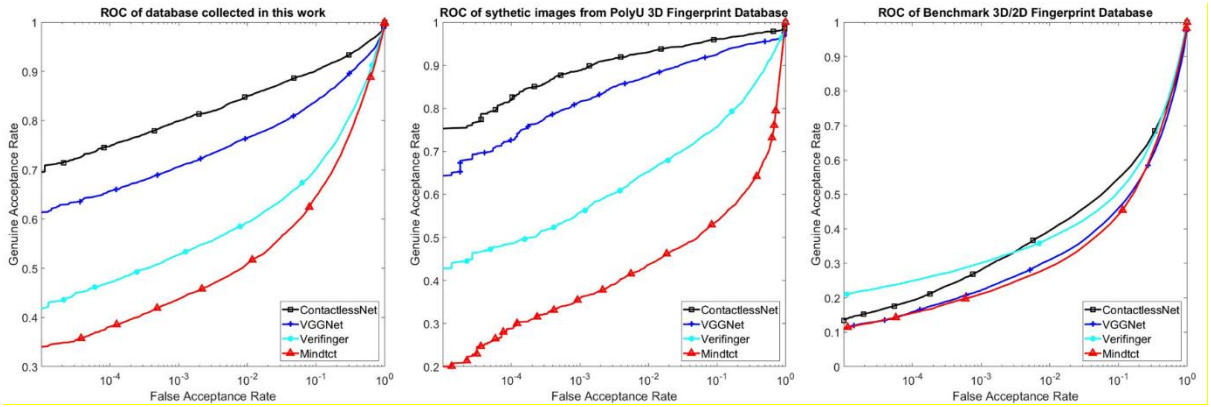

Figure 16: ROC for different databases and using different minutia extraction algorithms.

ROCs from these experiments are summarized in Figure 16. During the recognition experiments, one fingerprint image from each of the fingers, with least pose variation, is selected as the gallery, while of the images are employed for the query or as test samples. The

CMC plots from such experiments are shown in Figure 17.

Table 3: Equal error rates from different minutia extraction methods.

Database	Method	Equal Error Rate	AUC
Database acquired during this work [45]	MINDTCT	0.2523	0.8245
	Verifinger	0.2262	0.8524
	ContactlessNet	0.0995	0.9467
	VGG	0.1443	0.9140
PolyU Contactless Fingerprint Database [34]	MINDTCT	0.3643	0.7067
	Verifinger	0.1962	0.8769
	ContactlessNet	0.0484	0.9733
	VGG	0.0785	0.9506
Benchmark 2D/3D Fingerprint Database [35]	MINDTCT	0.3474	0.7124
	Verifinger	0.3263	0.7429
	ContactlessNet	0.3182	0.7439
	VGG	0.3663	0.7020

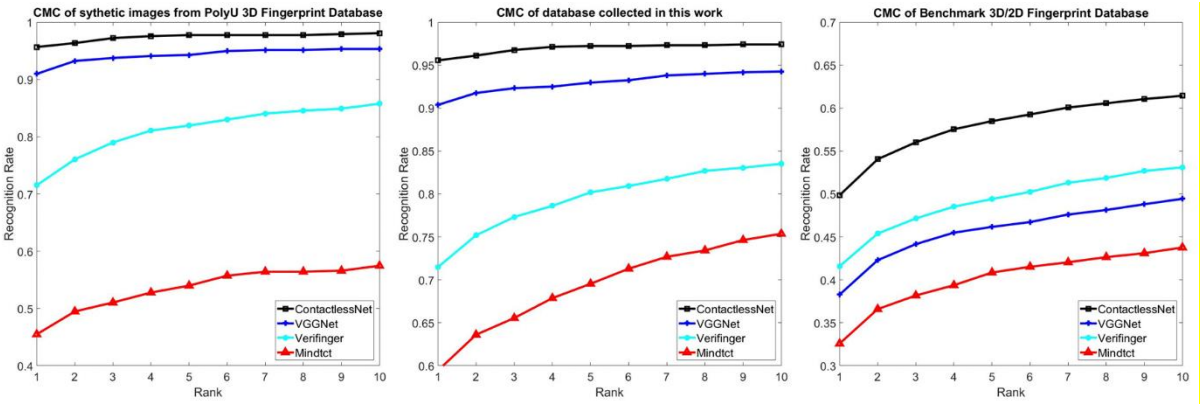

Figure 17: CMC for different databases and using different minutia extraction algorithms.

Table 4: Average rank-one recognition accuracy using different minutia extraction methods.

Database	Method	Rank-one accuracy
Database acquired during this work [45]	MINDTCT	0.5944
	Verifinger	0.7148
	ContactlessNet	0.9556
	VGG	0.9037
PolyU Contactless Fingerprint Database [34]	MINDTCT	0.4549
	Verifinger	0.7153
	ContactlessNet	0.9566
	VGG	0.9097
Benchmark 2D/3D Fingerprint Database [35]	MINDTCT	0.3258
	Verifinger	0.4159
	ContactlessNet	0.4986
	VGG	0.3828

Figure 18 presents sample minutiae extraction or localization results, and corresponding ground truth locations, from different image samples in three contactless fingerprint databases. The extraction time per image is around 0.8 second based on one GTX 1080TI.

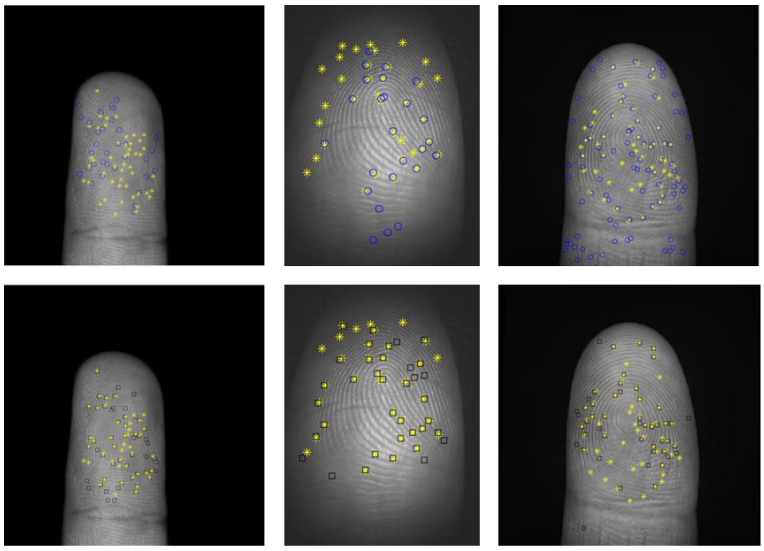

Figure 18: Sample contactless fingerprint images from three databases illustrating minutiae extraction results. The yellow star represents the ground truth, blue circles indicates the *Verifinger* prediction, black squares are predicted minutiae locations from *ContactlessNet*

4.3 Pose Compensation

The experimental results from the pose compensation approach detailed in section 2.3 are visually illustrated from the sample images in Figure 19, Figure 20, Figure 21, respectively from the database acquired during this work, database in [34], and in [35]. With the pose compensation approach, the image samples with different poses from same finger are better aligned or visually easy to recognize as compared with the raw images.

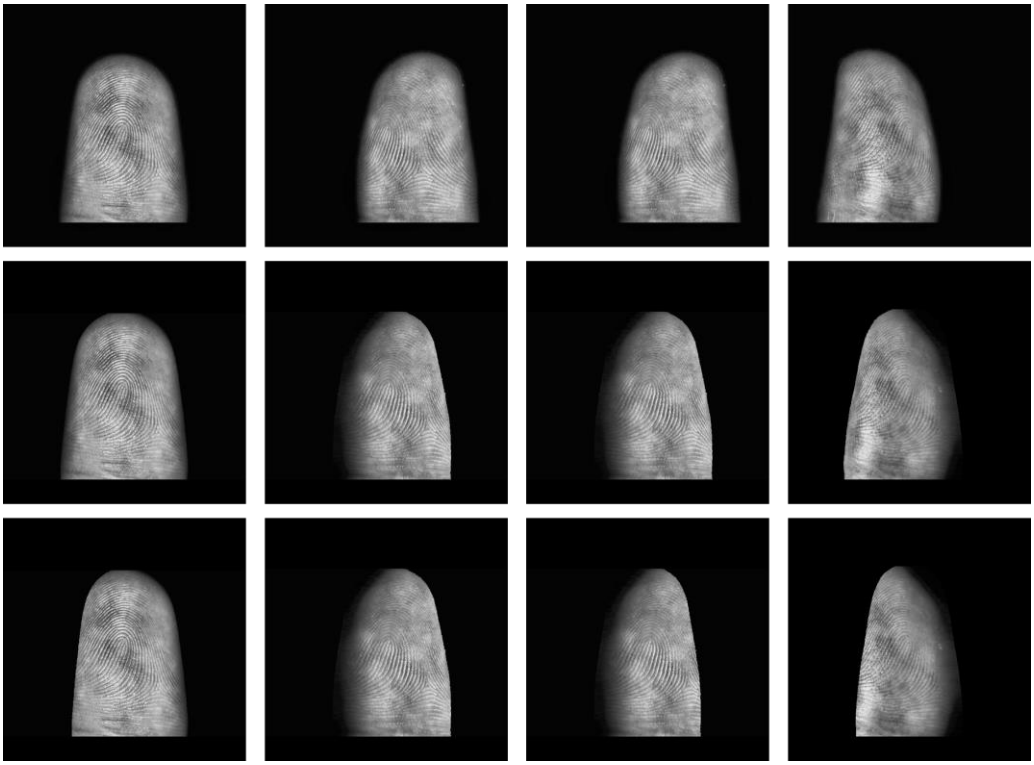

Figure 19: Sample pose compensation results using our database. Original contactless fingerprint images, the pose compensated images without the alignment and final pose compensation results are illustrated in top, middle and bottom rows respectively. First and second column are finger images with 0 and -40 deg view angles respectively. The third and fourth column are finger image with -40 and 40 deg view angles.

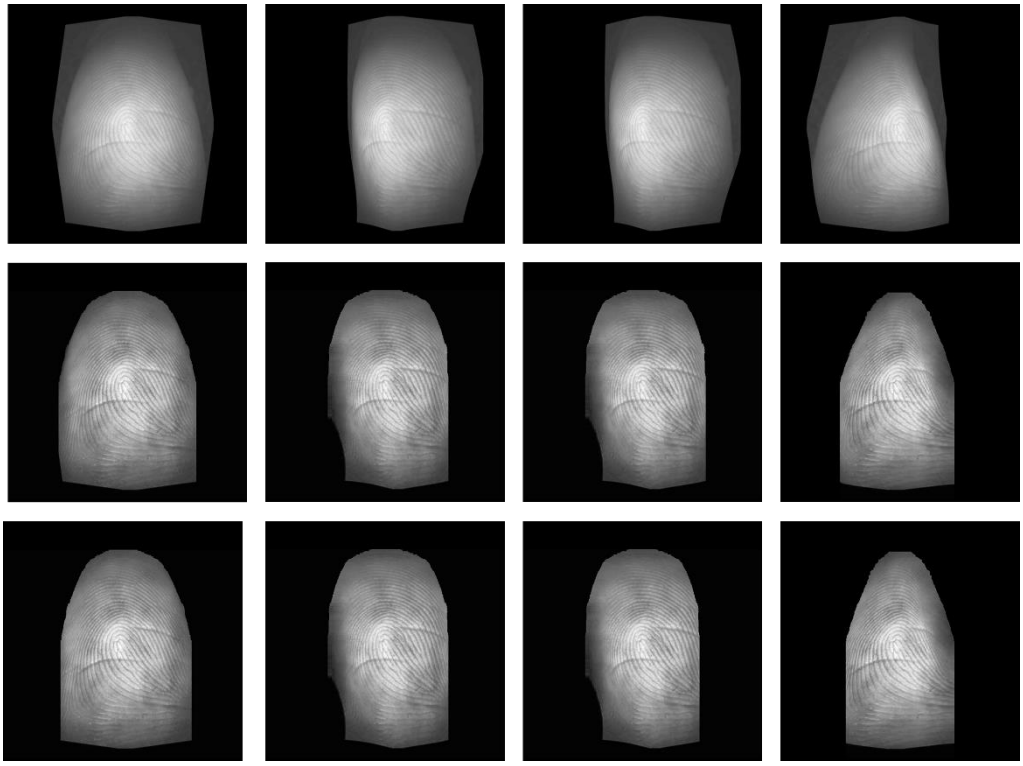

Figure 20: Sample pose compensation results using the images in database from [34], [42]. Original contactless fingerprint images, the pose compensated images without the alignment and final pose compensation results are illustrated in top, middle and bottom rows respectively. First and second column are finger images with 0 and -30 deg view angles respectively. The third and fourth column are finger image with -30 and 30 deg view angles.

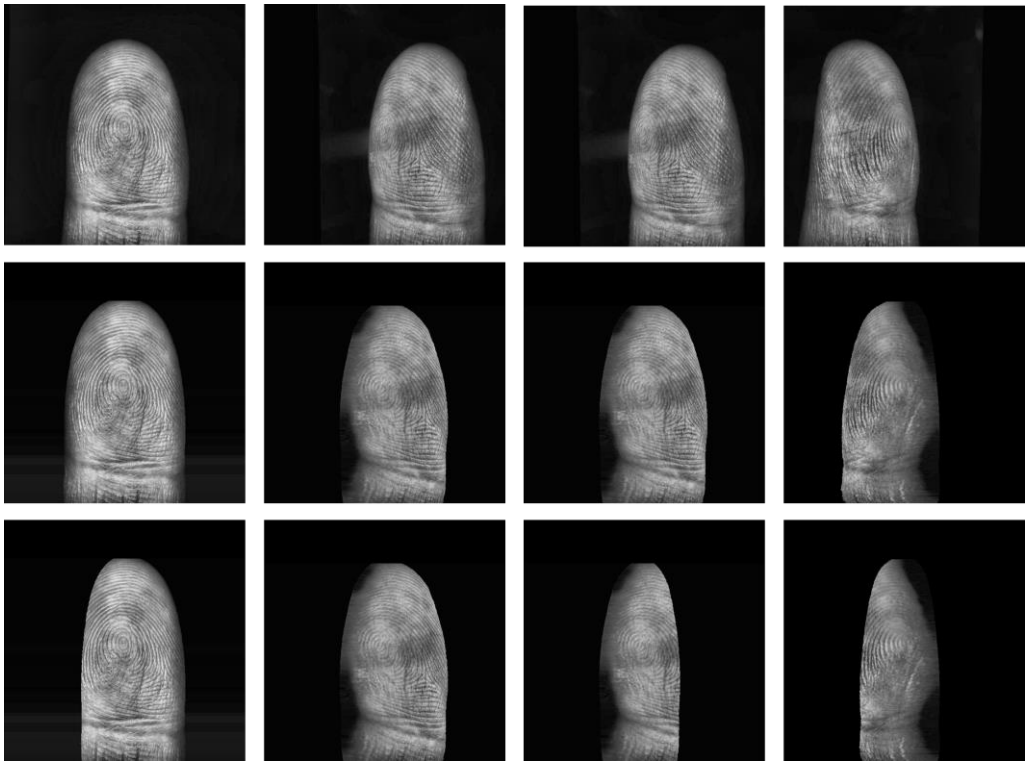

Figure 21: Sample pose compensation results from the database in [35]. Original contactless fingerprint images, the pose compensated images without the alignment and final pose compensation results are illustrated in top, middle and bottom rows respectively. First and second column are finger images with 0 and -60 deg view angles respectively. The third and fourth column are finger image with -60 and 60 deg view angles.

The verification performance from the pose compensation experiments are shown in Figure 22. The recognition performance using CMC is shown in Figure 23. We used same experiment protocols as in section 4.2. These results illustrate *MINDCT* representing the results using the minutiae extracted from NIST MINDCT [36], *Verifinger* representing the results using the minutiae extracted from *Verifinger* [15], the *ContactlessNet* represents the results using the minutiae extracted by *ContactlessNet*, while the *without alignment* represents the results using pure pose compensation with ellipsoid model and the *pose compensation* represents the results from the pose compensation with the alignment for different view angles.

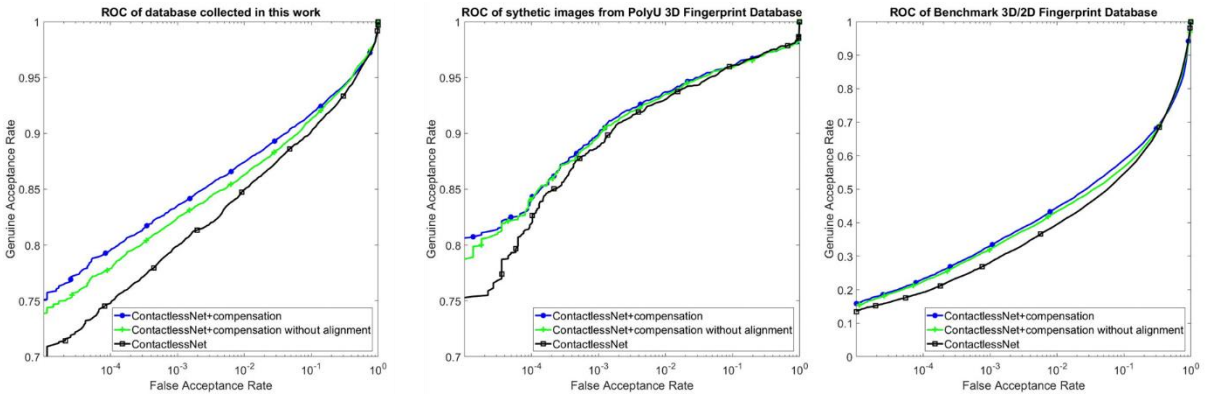

Figure 22: Comparative ROCs using different methods.

Table 5: Equal error rates using different correction methods.

Database	Method	Equal Error Rate	AUC
Database acquired during this work [45]	*ContactlessNet*	0.0995	0.9467
	ContactlessNet with pose compensation	0.0867	0.9527
	ContactlessNet no alignment	0.0887	0.9520
PolyU Contactless Fingerprint Database [34]	*ContactlessNet*	0.0484	0.9733
	ContactlessNet with pose compensation	0.0448	0.9729
	ContactlessNet no alignment	0.0473	0.9724
Benchmark 2D/3D Fingerprint Database [35]	*ContactlessNet*	0.3182	0.7439
	ContactlessNet with pose compensation	0.3237	0.7467
	ContactlessNet no alignment	0.3162	0.7467

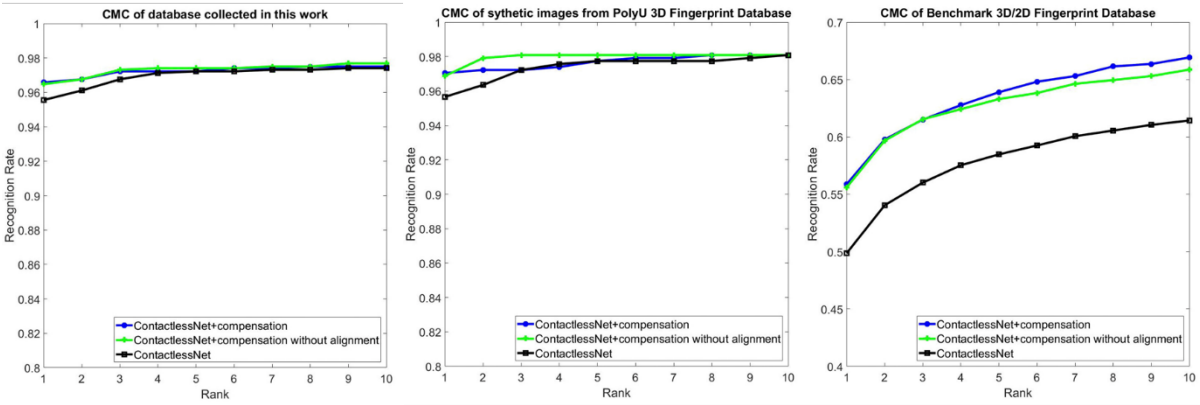

Figure 23: Comparative CMCs using different methods.

Table 6: Average rank one recognition accuracy using different correction methods.

Database	Method	Rank one
Database acquired during this work [45]	*ContactlessNet*	0.9556
	ContactlessNet with pose compensation	0.9657
	ContactlessNet no alignment	0.9648
PolyU Contactless Fingerprint Database [34]	*ContactlessNet*	0.9566
	ContactlessNet with pose compensation	0.9705
	ContactlessNet no alignment	0.9688
Benchmark 2D/3D Fingerprint Database [35]	*ContactlessNet*	0.4989
	ContactlessNet with pose compensation	0.5559
	ContactlessNet no alignment	0.5588

The method investigated in [28] incorporated the image-based compensation. Therefore to ensure fairness in the comparison, the proposed correction method is adapted to image version as summarized in Algorithm 3 with alignment. The verification and recognition experimental results, using the *Verifinger* matcher, are shown in Figure 24, Figure 25.

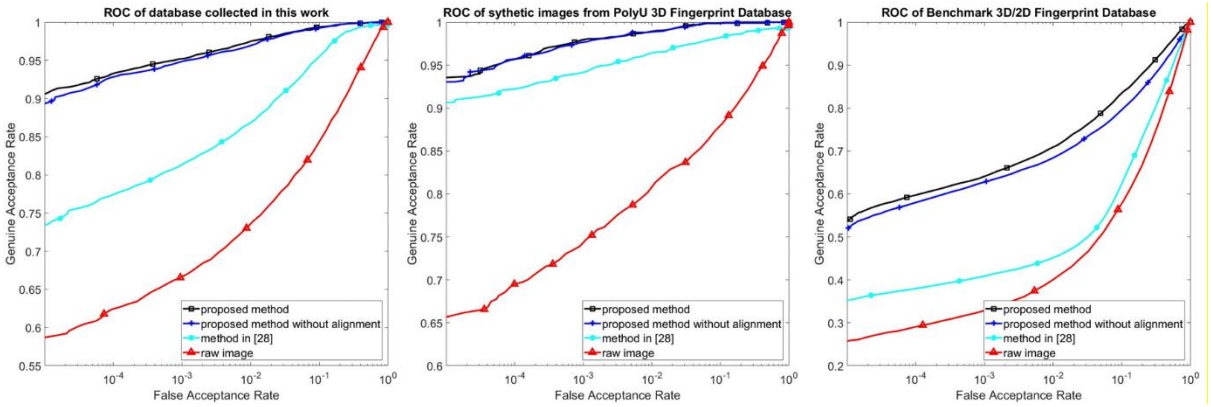

Figure 24: Comparative ROCs from different databases using from our method and method in [28].

Table 7: Equal error rates of different methods using *Verifinger*.

Database	Method	Equal Error Rate	AUC
Database acquired during this work [45]	Original image	0.1364	0.9366
	Proposed method	0.0195	0.9975
	Proposed method no alignment	0.0217	0.9972
	Method based on [28]	0.0634	0.9840
PolyU Contactless Fingerprint Database [34]	Original image	0.1161	0.9466
	Proposed method	0.0105	0.9991
	Proposed method no alignment	0.0106	0.9994
	Method based on [28]	0.0284	0.9895
Benchmark 2D/3D Fingerprint Database [35]	Original image	0.2785	0.8063
	Proposed method	0.1427	0.9301
	Proposed method no alignment	0.1673	0.9063
	Method based on [28]	0.2408	0.8416

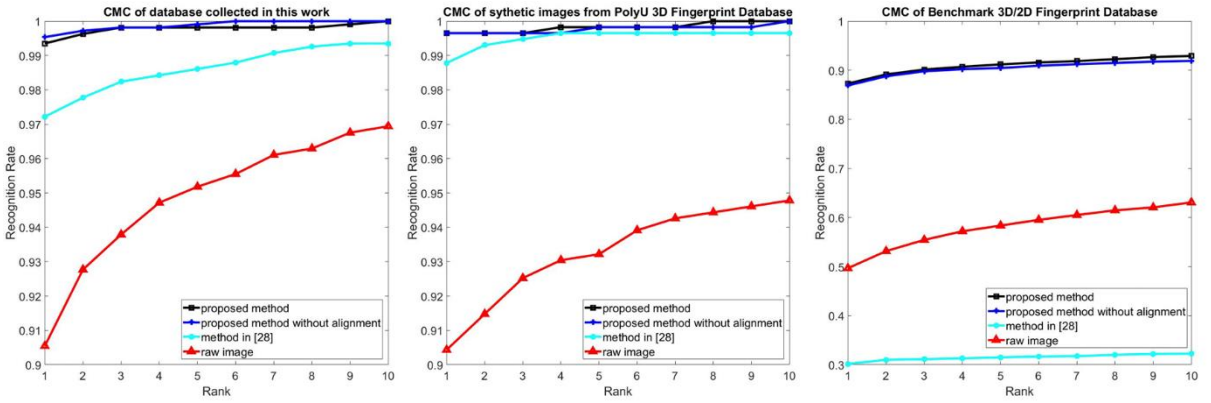

Figure 25: Comparative CMCs from different databases using from our method and method in [28].

Table 8: Average rank-one recognition accuracy from different pose compensation methods.

Database	Method	Rank-one accuracy
Database acquired during this work [45]	Original image	0.9055
	Proposed method	0.9935
	Proposed method no alignment	0.9954
	Method based on [28]	0.9722

Polyu Contactless Fingerprint Database [34]	Original image	0.9043
	Proposed method	0.9965
	Proposed method no alignment	0.9965
	Method based on [28]	0.9878
Benchmark 2D/3D Fingerprint Database [35]	Original image	0.4967
	Proposed method	0.8729
	Proposed method no alignment	0.8691
	Method based on [28]	0.3017

4.4 Discussion

Our experimental results for the contactless fingerprint minutiae detection, presented in previous section, indicates that the proposed *ContactlessNet* approach can achieve F1 score of 0.741, 0.628, 0.672 on three different or public databases. During the identification experiments, the rank-one accuracy increases from 0.7148, 0.7153, 0.4159 (*Verifinger*) to 0.9556, 0.9566, 0.4986 on three respective databases. As for the verification experiments, *ContactlessNet* also helps to improve the performance, or decreases the EER and improves AUC, for the database acquired in this work and database from [34]. However, for the database from [35], different extraction methods do not show any appreciable differences in the verification performance and this can be attributed to the extreme pose changes among the contactless fingerprints images available from this database.

The pose compensation method also achieves some improvements in the verification performance from the extracted minutiae, *i.e.*, 10.85%, 2.27%, 0.63% decrease in the EER among three respective databases. In addition, some performance improvement can also be observed by incorporating pose alignment between the different view angle images

Our experimental results for the identification problem similarly achieve small but consistent improvements even for the databases that do not have large view angle differences in their contactless fingerprint images. However for the database in [35] which illustrate images with extreme view angle differences, we can observe 11.43% improvement, over the use of only raw extracted minutiae. Inherited error in the contactless fingerprint minutiae extraction contributes to the unremarkable improvement in the performance using the proposed pose compensation and alignment method. Our experimental results demonstrate impressive performance improvement using the *Verifinger* matcher, *i.e*. 84.09%, 90.96%, 39.93% decrease in EER and 9.93%, 10.20%, 74.97% improvement in the rank-one accuracy for three respective databases by incorporating pose compensation as compared to the raw images. Similarly we

can also observe 10.14%, 0.94%, 14.70% decrease in the EER values with the usage of alignment approach as compared to the pose compensated image. Therefore, these experimental results consistently indicate that the pose compensation and alignment approach introduced in section 2 is very effective, especially on the contactless fingerprint database with large pose difference images.

For large varieties in pose of fingerprint image, a polynomial model in [28] cannot adequately capture the shape changes. As shown from sample contactless fingerprint images in Figure 26, in the top row image sample, when the view angle of the image is relatively small, the method in [28] can help to alleviate the deformation to certain extent. However, when such view angle is significantly large, as shown from the image sample in the bottom row, the approach in [28] cannot handle the distortion and the compensation results are far from being satisfactory. The observed equal error rates are relatively high while using the MCC matcher. However, as can be observed from the results in Table 7 , theses equal error rate is also high when we directly use *Verifinger* matcher. This can be attributed to the nature of the database and as significant changes in the pose or the sensor view angle can significantly degrade the contactless fingerprint matching accuracy. Generation of contactless fingerprint images with synthetic poses has also been incorporated in earlier references, *e.g*. [46]. However, our method is completely different from [46], *i.e*., our work in on contactless 2D fingerprint recognition while [46] is on 3D fingerprints, [46] does not make any attempt to compensate the pose but generates nine templates for different poses by rotating the acquired 3D fingerprint while we estimate the pose from a *single* 2D image and specifically compensate it into front-view image by 3D rotation of proposed ellipsoid model, *etc*.

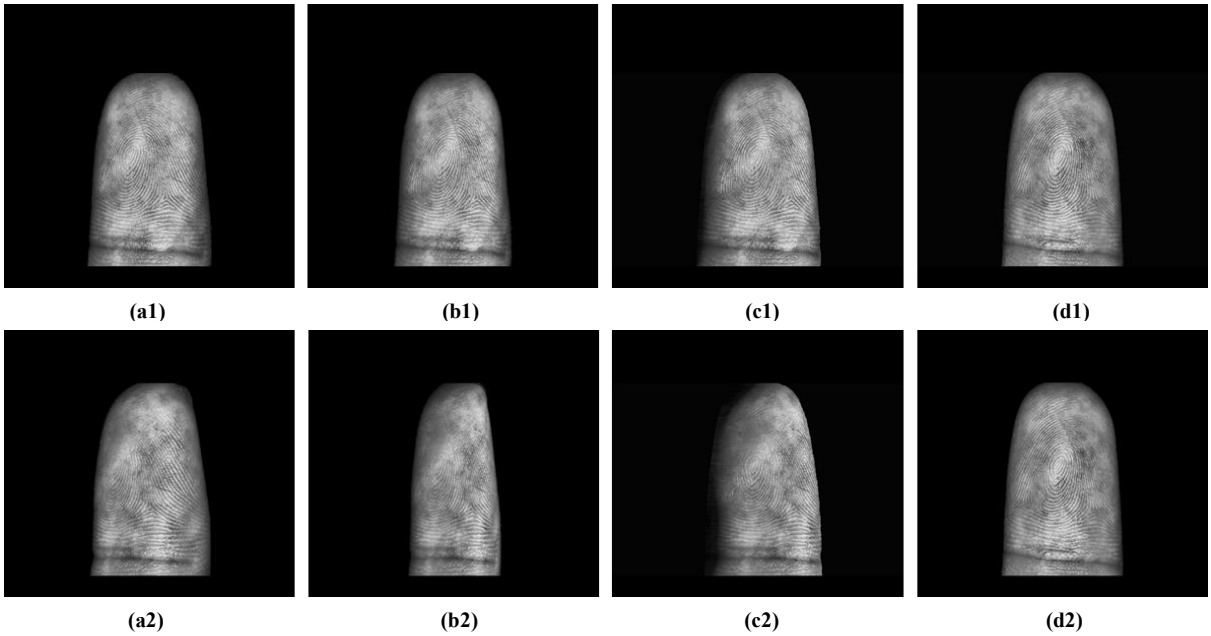

Figure 26: Visualization of sample fingerprints pose compensation results: (a1)-(a2) acquired fingerprint samples from arbitrary pose; (b1)-(b2) pose compensation results using [28]; (c1)-(c2) our results; (d1)-(d2) front view images for samples in (a1)-(a2).

5. Conclusions and Further Work

This paper has developed a new approach for contactless fingerprint minutiae detection using deep neural network that incorporates atrous spatial pyramid pooling. Our reproducible experimental results [45] presented in this paper suggest promising improvement in the performance using the proposed architecture. This paper also presents the cross-database contactless fingerprint performance evaluation that trains the network using the images acquired during this work and the performance is evaluated using the two other public databases, without incorporating any fine-tuning. Such cross-database performance evaluation results presented in section 4 also helps to further validate the effectiveness and robustness of the presented framework.

Despite promising results from the contactless 2D fingerprint minutiae extraction and pose-invariant recognition investigated in this work, an image-based instead of patch-based *ContactlessNet* is expected to be computationally economical and therefore preferred. However to achieve such objective, additional labelled (ground truth) contactless fingerprint images are required to further improve minutiae extraction results especially for the low quality regions generally observed near the boundary. In addition, the generative adversarial networks have the potential to directly perform face fractalization with self-learnt features. Such method can be explored for the contactless fingerprint pose compensation and is part of further work in this area.

6. References

[1] D. Maltoni, D. Maio, A. K. Jain, and S. Prabhakar, *Handbook of Fingerprint Recognition*. Springer Science & Business Media, 2009.

[2] S. Yoon and A. K. Jain, "Longitudinal study of fingerprint recognition," *Proc. National Academy of Sciences*, vol. 112, no. 28, pp. 8555-8560, 2015.

[3] A. M. Bazen and S. H. Gerez, "Fingerprint matching by thin-plate spline modelling of elastic deformations," *Pattern Recognition*, vol. 36, no. 8, pp. 1859-1867, 2003.

[4] R. Cappelli, D. Maio, and D. Maltoni, "Modelling plastic distortion in fingerprint images," *Proc. Intl. Conf. Advances in Pattern Recognition*, Springer, pp. 371-378, 2001.

[5] A. Ross, S. Dass, and A. K. Jain, "A deformable model for fingerprint matching," *Pattern Recognition*, vol. 38, no. 1, pp. 95-103, 2005.

[6] G. Parziale, "Touchless Fingerprinting Technology," *Advances in biometrics*, Springer, pp. 25-48. 2008.

[7] Y. Song, C. Lee, and J. Kim, "A new scheme for touchless fingerprint recognition system," *Proc. Intl. Symp. Intell. Signal Processing and & Comm. Systems*, ISPACS 2004. pp. 524-527. 2004.

[8] C. Lee, S. Lee, and J. Kim, "A study of touchless fingerprint recognition system," *Proc. Joint IAPR International Workshops on Statistical Techniques in Pattern Recognition (SPR) and Structural and Syntactic Pattern Recognition (SSPR)*, pp. 358-365. Springer, 2006.

[9] G. Parziale and Y. Chen, "Advanced technologies for touchless fingerprint recognition, *Handbook of Remote Biometrics*, Springer, pp. 83-109, 2009.

[10] B. Y. Hiew, A. B. Teoh, and Y.-H. Pang, "Touch-less fingerprint recognition system," *Proc. IEEE Workshop on Automatic Identification Advanced Technologies*, AutoID07, pp. 24-29, 2007.

[11] A. Kumar and Y. Zhou, "Contactless fingerprint identification using level zero features," *Proc. CVPR 2011 Biometrics Workshop*, pp. 114-119, 2011.

[12] A. Sankaran, A. Malhotra, A. Mittal, M. Vatsa, and R. Singh, "On smartphone camera based fingerphoto authentication," *Proc. BTAS*, pp. 1-7, 2015.

[13] A. Malhotra, A. Sankaran, A. Mittal, M. Vatsa, and R. Singh, "Fingerphoto authentication using smartphone camera captured under varying environmental conditions," in *Human Recognition in Unconstrained Environments*, Ch. 6, pp. 119-144, Academic Press, 2017.

[14] C. Stein, C. Nickel, and C. Busch, "Fingerphoto recognition with smartphone cameras," *Proc. BIOSIG 2012*, pp. 1-12, 2012.

[15] VeriFinger, S.D.K. Neuro Technology, VeriFinger, S. D. K. Neuro Technology. Dec. 2017.

[16] A. Farina, Z. M. Kovacs-Vajna, and A. Leone, "Fingerprint minutiae extraction from skeletonized binary images," *Pattern Recognition*, vol. 32, no. 5, pp. 877-889, 1999.

[17] L. Hong, Y. Wan, and A. Jain, "Fingerprint image enhancement: Algorithm and performance evaluation," *IEEE Trans. Pattern Anal. Mach. Intell*., vol. 20, no. 8, pp. 777-789, 1998.

[18] S. Chikkerur, A. N. Cartwright, and V. Govindaraju, "Fingerprint enhancement using STFT analysis," *Pattern Recognition*, vol. 40, no. 1, pp. 198-211, 2007.

[19] D. Maio and D. Maltoni, "Direct gray-scale minutiae detection in fingerprints," *IEEE Trans. Pattern Anal. Mach. Intell*., no. 1, pp. 27-40, 1997.

[20] V. K. Sagar and K. J. B. Alex, "Hybrid fuzzy logic and neural network model for fingerprint minutiae extraction," *Proc. IEEE Intl. J. Conf. Neural Networks*, IJCNN'99, vol. 5, pp. 3255-3259, 1999.

[21] X. Jiang, W.-Y. Yau, and W. Ser, "Detecting the fingerprint minutiae by adaptive tracing the gray-level ridge," *Pattern Recognition*, vol. 34, no. 5, pp. 999-1013, 2001.

[22] H. Jiang and M. Liu, "Fingerprint minutiae detection based on multi-scale convolution neural networks," *Proc. Chinese Conf. Biometric Recognition*, Springer, pp. 306-313, 2017.

[23] L. Jiang, T. Zhao, C. Bai, A. Yong, and M. Wu, “A direct fingerprint minutiae extraction approach based on convolutional neural networks,” *Proc. IEEE Intl. J. Conf. Neural Networks*, IJCNN 2016, pp. 571-578, 2016.
[24] Y. Tang, F. Gao, J. Feng, and Y. Liu, “FingerNet: An unified deep network for fingerprint minutiae extraction,” *Proc. IJCB 2017*, pp. 108-116, Denver, 2017.
[25] Y. Tang, F. Gao, and J. Feng, “Latent fingerprint minutia extraction using fully convolutional network,” *Proc. IJCB 2017*, Denver, pp. 117-123, 2017.
[26] D.-L. Nguyen, K. Cao, and A. K. Jain, “Robust minutiae extractor: Integrating deep networks and fingerprint domain knowledge,” *Proc. Intl. Conf. Biometrics*, ICB 2018, Gold Coast, pp. 9-16, 2018.
[27] X. Yin, J. Hu, and J. Xu, “Contactless fingerprint enhancement via intrinsic image decomposition and guided image filtering,” *Proc. 11th IEEE Conf. Industrial Electronics and Applications (ICIEA)*, pp. 144-149, 2016.
[28] R. D. Labati, A. Genovese, V. Piuri, and F. Scotti, “Contactless fingerprint recognition: a neural approach for perspective and rotation effects reduction,” *Proc. IEEE Workshop Computational Intell. in Biometrics and Identity Management (CIBIM)*, pp. 22-30, 2013.
[29] T. Hassner, S. Harel, E. Paz, and R. Enbar, “Effective face frontalization in unconstrained images,” *Proc. IEEE Conf. Computer Vision & Pattern Recognition*, pp. 4295-4304, 2015.
[30] X. Yin, X. Yu, K. Sohn, X. Liu, and M. Chandraker, “Towards large-pose face frontalization in the wild,” *Proc. ICCV, 2017*, pp. 1-10, Venice, Oct. 2017.
[31] R. Cappelli, D. Maio, and D. Maltoni, “SFinGe: an approach to synthetic fingerprint generation,” *Proc. Intl. Workshop Biometric Technologies (BT2004)*, pp. 147-154, 2004.
[32] P. Schuch, S. Schulz, and C. Busch, “Minutia-based enhancement of fingerprint samples,” *Proc. IEEE Intl. Carnahan Conf. Security Technology* (ICCST), pp. 1-6, 2017.
[33] L.-C. Chen, G. Papandreou, I. Kokkinos, K. Murphy, and A. L. Yuille, “Deeplab: Semantic image segmentation with deep convolutional nets, atrous convolution, and fully connected crfs” *IEEE Trans. Pattern Anal. Mach. Intell*., vol. 40, no. 4, pp. 834-848, 2018.
[34] C. Lin and A. Kumar, “Tetrahedron based fast 3D fingerprint identification using colored LEDs illumination,” *IEEE Trans. Pattern Anal. Mach. Intell*., vol. 40, no. 12, pp. 3022-3033, 2018.
[35] W. Zhou, J. Hu, I. Petersen, S. Wang, and M. Bennamoun, “A benchmark 3D fingerprint database,” *Proc. 11th Intl. Conf. Fuzzy Systems and Knowledge Discovery (FSKD)*, pp. 935-940, 2014.
[36] K. Ko, "User's guide to NIST biometric image software (NBIS)," 2007.
[37] C. Lin and A. Kumar. “Matching contactless and contact-based conventional fingerprint images for biometrics identification,” *IEEE Trans. Image Process*., vol. 27, pp. 2008–2021, April 2018.
[38] D. Maio, D. Maltoni, R. Cappelli, J. L. Wayman, and A. K. Jain, “FVC2002: Second fingerprint verification competition,” *Proc. ICPR 2002*, vol. 3, pp. 811-814, 2002.
[39] C. I. Watson and C. Wilson, *NIST Special Database 4: Fingerprint Database*, National Institute of Standards and Technology, vol. 17, p. 77, 1992.
[40] S. M. Pizer, E. P. Amburn, J. D. Austin, R. Cromartie, A. Geselowitz, T. Greer, B. ter Haar Romeny, J. B. Zimmerman, and K. Zuiderveld, “Adaptive histogram equalization and its variations,” *Proc. Computer Vision, Graphics, & Image Processing*, vol. 39, no. 3, pp. 355–368, 1987.
[41] C. Lin and A. Kumar, “Contactless and partial 3D fingerprint recognition using multi-view deep representation,” *Pattern Recognition*, vol. 83, pp. 314-327, 2018.
[42] K. Simonyan and A. Zisserman, "Very deep convolutional networks for large-scale image recognition," arXiv preprint arXiv:1409.1556, 2014.
[43] A. Paszke, S. Gross, S. Chintala, and G. Chanan, "PyTorch," ed, 2017.

[44] R. Cappelli, M. Ferrara, and D. Maltoni, “Minutia cylinder-code: A new representation and matching technique for fingerprint recognition,” *IEEE Trans. Pattern Anal. Mach. Intell*., vol. 32, no. 12, pp. 2128-2141, 2010.
[45] Weblink to download Contactless Fingerprint Database from this paper and codes for the reproducibility, http://www.comp.polyu.edu.hk/~csajaykr/CFPose,zip, 2019.
[46] R. D. Labati, A. Genovese, V. Piuri, and F. Scotti, “Toward unconstrained fingerprint recognition: a fully-touchless 3-D system based on two views on the move,” *IEEE Trans. Sys. Man, and Cybern.: Systems*, vol. 46, no. 2, pp. 202-219, Feb. 2016.